Renewable Energy 172 (2021) 477–487

Contents lists available at ScienceDirect

Renewable Energy

journal homepage: www.elsevier.com/locate/renene

A study on heat transfer enhancement for solar air heaters with ripple surface

Zhimin Dong, Peng Liu, Hui Xiao, Zhichun Liu, Wei Liu*

School of Energy and Power Engineering, Huazhong University of Science and Technology, 1037 Luoyu Road, Wuhan, 430074, China

ARTICLE INFO

Article history:
Received 20 November 2020
Received in revised form
9 March 2021
Accepted 10 March 2021
Available online 13 March 2021

Keywords:
Solar air heater
Longitudinal vortices
Heat transfer enhancement
Pressure drop
Turbulent flow

ABSTRACT

Flat-Plate solar air heater (SAH) is utilized widely to relieve the fossil energy crisis nowadays. With the aim to improve the efficiency of the devices, heat transfer and flow characteristic in a solar air heater with novel inclined groove ripple surfaces were investigated in this work. The effect of three different parameters, such as groove amplitude, attack angle, and array number, on the overall performance of air heater was analyzed in the range of Reynolds number from 12000 to 24000. The inclined grooves on the ripple surface have a significant impact on the working fluid for generating longitudinal swirl flow in the duct of air heater, which mixes the air to enhance heat transfer, $Nu/Nu_0 = 1.21-3.38$, and leads to a moderate increase of pressure drop in the same time, $f/f_0 = 1.54-6.96$. The solar air heater composed with ripple surface is of excellent overall thermo-hydraulic performance, Nusselt numbers are 1.04–1.94 times higher than the smooth duct at same blowing energy consumption.

1. Introduction

Solar energy is qualitatively superior and quantitatively abundant to fulfill the energy needs of the modern life with low negative environmental impacts. Advanced solar energy utilization technology requires high-grade energy to achieve the most efficient application, and the parabolic trough collector has the capability to meet thermal energy and electrical demands [1]. Thermochemical reactions involved in endothermic reactions can make use of concentrated solar irradiation as the energy source for high-temperature processed heat and the maximum temperature in such a kind of reactors can reach 1500K or higher [2]. In low temperature range, solar air heater, as one of the simplest and most economical devices, is extensively used for many applications at low temperature, such as space heating and cooling, solar chimneys, refrigeration and dryers and so on [3].

However, the low efficiency restricts the development of flat-plate solar air heaters. Lots of heat transfer enhancement techniques have been investigated to improve the performance of the collectors. The dominant method is pecking turbulence promoters and the most popular turbulators including ribs, grooves, fins, baffles, wings, winglets, and conical strip inserts [4]. The mechanism of the turbulators to enhance heat transfer is that they break the viscous sublayer, increase the turbulent intensity or heat transfer area, and generate vortices or secondary flows. For a long time, hundreds of thousands of artificially roughened surfaces have been studied [5]. R.P. Saini carried out experiments to analyze the heat transfer and friction factor of the collectors pecked by dimple-shape roughened surface [6]. Absorber surfaces fixed by ribs with different transverse section shapes and different arrangements have been investigated by many researchers. PEC, which is defined as $(Nu/Nu_0)/(f/f_0)^{(1/3)}$, is an overall criterion to evaluate the performances of heat transfer equipment. Yadav found that the collector with the square sectioned transverse ribs can achieve a high overall thermo-hydraulic performance with *PEC* value reaching to 1.88 when Reynolds number is 12000 [7]. Many other ribs and their best overall thermo-hydraulic performance can be abstracted as follow: winglets combined with wavy grooves, $PEC = 2.12$ [8]; conical protrusion roughness ribs, efficiency enhancement factor of which reaches to 1.346 [9]; ribs combined downstream half-size or same-size ribs, $(Nu/Nu_0)/(f/f_0) = 0.74$ [10]; criss-cross rib patterns, $PEC = 1.5$ [11]; and other sixteen kinds of cross-sectional shapes have been compared by Mi-Ae Moon [12].

Furthermore, irreversibility of heat transfer and mechanical energy consumption for a convective heat transfer process was evaluated by theories such as exergy destruction [13,14] and entropy generation [15]. Based on the exergy destruction minimization principle, Xiao et al. conducted an investigation on seeking out

* Corresponding author.
E-mail address: w_liu@hust.edu.cn (W. Liu).

https://doi.org/10.1016/j.renene.2021.03.042
0960-1481/

optimal flow structure for convective heat transfer in the duct [16]. They found that longitudinal swirl flows behave pretty well in the irreversibility.

Skullong et al. [17] studied the thermal performance of flat plate solar air heaters fitted with two kinds of winglet-type vortex generators. It was found that thermal enhancement factor value of the perforated-trapezoidal winglet-type vortex generators are around 3.65%–6.34% higher than that of perforated-rectangular winglet-type vortex generators. They have proposed many other efficacious methods for enhancing heat transfer, such as V-baffle vortex generators [18], wavy-groove and perforated-delta wing vortex generators [19], rib-groove turbulators [20], Delta Winglet Vortex Generator [21], ribs [22], winglets and wavy grooves [8], hole-punched wings [23], etc. Jin, a Chinese researcher, carried out a numerical investigation of SAH fixed with similar multiple V-shaped ribs. They also found that the longitudinal swirl flows are generated, which are beneficial to improve the heat transfer rate [24,25]. Moreover, lots of inserts like inclined circle or rectangle rods, may help generate counter-rotating vortices [26,27]. Therefore, the techniques can be employed to flat-plate solar air heaters too.

As a kind of advanced technique, nanofluids are considered to improve the performance of thermal equipment greatly. Combination of dispersed Al_2O_3 and water performs wall in reducing the irreversibility of the solar collectors with turbulator [28]. Remarkable achievement in nanofluid technique exploration has been realized by Prof. Sheikholeslami, and the paper published by their lab has proved that the using of nanomaterial and helical tapes reduces the entropy generation by 89.98% in the tube side of heat exchangers [29]. CuO nanomaterial has been dispersed into H_2O to help its conductivity, and double twisted tapes have been installed to realize the minimum irreversibility [30]. Moreover, nanofluid with particles such as copper, alumina, titanium oxide has a positive impact on the heat transfer performance when the magnetic field was employed [31]. Nanofluid is an invaluable novel technique which will be employed in heat transfer enhancement more and more in future.

The heat transfer and friction factor of a solar air heater composed with a corrugated surface were experimentally investigated by Gao [32] and Singh [33]. It was found that secondary flows are produced when the air flows across the grooves perpendicularly, which are conducive to improving heat transfer performance. However, air from near-wall and core regions can't mix completely. In order to further improve the heat transfer rate, a type of improved solar air heater composed with inclined ripple surface is proposed and numerically studied in this paper. The inclined ripple surface is expected to form longitudinal swirl flows in the duct to enhance the air mixing between the region near wall and core region. Consequently, the overall thermo-hydraulic performance of the SAHs is expected to be significantly improved.

2. Physical model

2.1. Geometric model

A typical flat-plate solar energy collecting system is shown in Fig. 1, and the geometric models of the SAHs are shown in Fig. 2. When solar radiation passes through a transparent cover and impinges on the blackened absorber surface of high absorptivity, a large portion of this energy is absorbed by the plate and then transferred to the transport medium, air, in the collector to be carried away for heating the room.

As far as the solar air heater concerned in this paper, an upstream section of 200 mm in length is arranged in the SAH model to make sure that the fully developed air turbulence flows into the test section, whose length is 500 mm, and a downstream section with the length of 100 mm connects with the test section. The width and the height of the collectors are respectively 160 mm and 20 mm. The longitudinal cross-section of the corrugated surface is a sinusoidal curve with three amplitude values ($A = 1$ mm, 1.5 mm, 2 mm) and the period length (P) is fixed as 20 mm. Parameters studied are shown in Table 1.

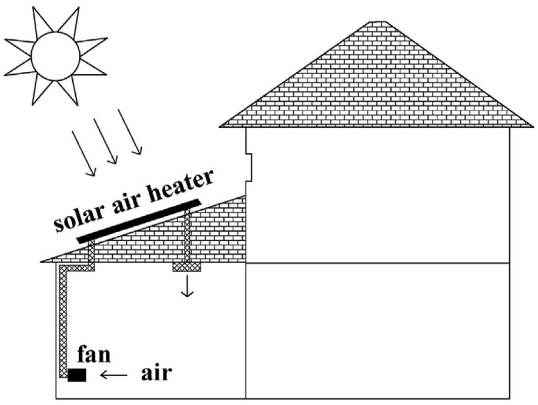

Fig. 1. Solar energy collecting system.

The attack angles (α) of the corrugated surface with respect of the main flow direction are separately set to four values (45°, 60°, 75°, and 90°). The heated surface is divided into 2, 4, 6 or 8 parts, and it can also be considered composed by symmetrical inclined parts, as shown in Fig. 2. When the attack angle is smaller than 90°, the groove direction is not perpendicular to the bulk flow. The aim of those surface distributions is to induce the fluid to flow in different directions and generate numerous longitudinal swirl flows.

2.2. Mesh model

The geometric model is divided into tens of millions of elements to adjust to the simulation conditions. Hexahedra grid is used to fulfill the core region, aiming to reduce the computation resource requirements. In order to realize the simulation of flow situations in the boundary layer, highly dense grid with twenty layers of prism grid are set near the walls. In the meanwhile, tetrahedron and pyramid mesh is employed to connect the prism and hexahedra grid as shown in Fig. 3.

2.3. Boundary conditions

Air is chosen as the test fluid in the present work. The physical properties are listed in Table 2 and the fluid flowing through the ducts is considered to be steady-state.

The test fluid (air), flowing through the duct with Reynolds number (Re) ranging from 12000 to 24000, gives a fully turbulent condition and takes the thermal energy away from the heated surface. Ambient temperature of 300K is set to the inlet boundary.

As shown in Fig. 4, when solar radiation (about 1000 W/m^2) passes through a transparent cover, around 7% of the energy is reflected to the environment by the first glass. The rest cover and the bottom surface have similar reflection coefficient, and finally, there is about 804.36 J solar energy, in per second and at per square meter, will be converted into heat by the blackened absorber surface. Thus, in this paper, the heated wall is subjected to an approximately uniform heat flux of 800W/m^2. Meanwhile, a heat insulated condition is set to the remaining walls. Since the honeycombs and multiple glass covers are employed to efficiently

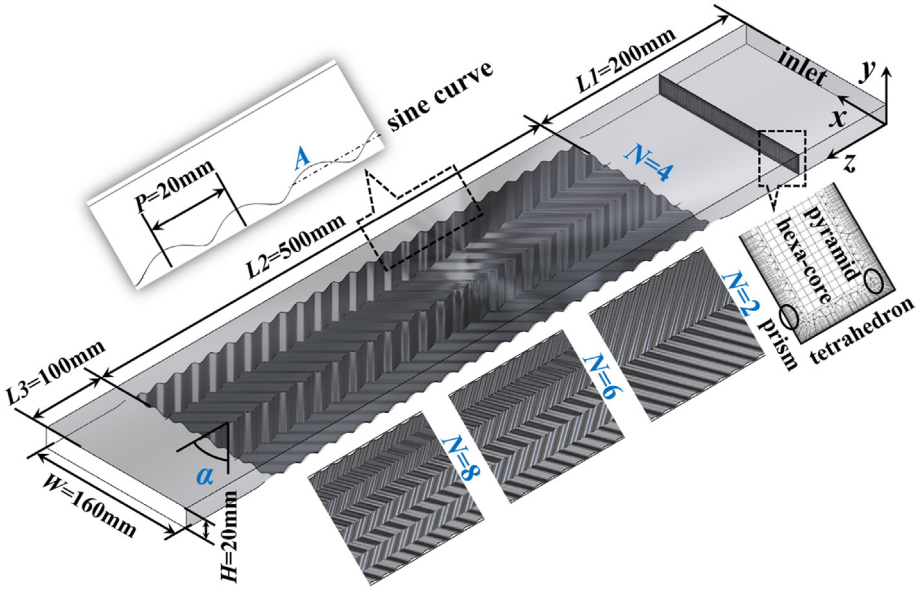

Fig. 2. Schematic diagram of the E-SAHs composed with inclined ripple surfaces.

Table 1
Parameters studied and the value ranges of them.

parameters	*A* (mm)	*α* (°)	*N*
values	1, 1.5, 2	90, 75, 60, 45	2, 4, 6, 8

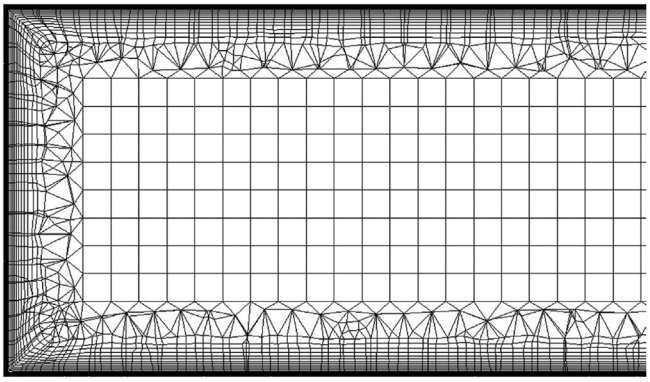

Fig. 3. A view of partial mesh of solar air heater section.

Table 2
The physical properties of the air.

density ρ kg/m^3	thermal conductivity λ W/(m·k)	dynamic viscosity μ kg/(m·s)	specific heat c_p J/(kg·k)
1.225	0.0242	1.789×10^{-5}	1006.43

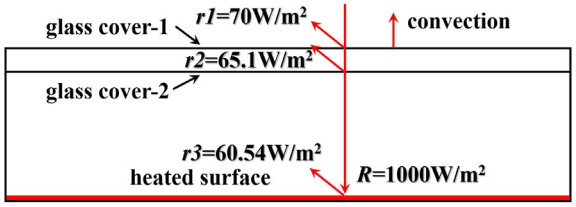

Fig. 4. Boundary condition model.

suppress the re-radiation and the convection losses from the collectors to the environment [34]. In this paper, a thermo-isolated boundary condition is adopted to replace the multiple glass covers approximately.

The numerical investigation is carried out by ANSYS Fluent 15.0 software which is based on finite volume method and SIMPLE algorithm is employed to couple pressure and velocity. The spatial discretization is set as Second Order Upwind format for momentum, turbulent kinetic energy, and specific dissipation rate and so on. SST *k*-*ω* model is chosen to deal with the iterations in turbulence flow process.

2.4. Simulation parameters

The Reynolds number, which depicts the flow situation, is defined by the following equation:

$$Re = \frac{\rho V D_e}{\mu} \tag{1}$$

where V is the bulk velocity of the fluid, and D_e is the equivalent diameter of the ducts, which is calculated by $D_e = 4WH/2(W+H)$. Reynolds numbers and their respective mass flow rate are recorded in the Table 3.

The average convection heat transfer coefficient and the Nusselt number are respectively defined by:

$$h = \frac{q}{T_w - T_m} \tag{2}$$

$$Nu = \frac{hD_e}{k} \tag{3}$$

where T_w and T_m represent the average temperature of the heated wall and the bulk fluid.

Table 3
Reynolds numbers and respective mass flow rates (marked as m).

Re	12000	15000	18000	21000	24000
***m* (kg/s)**	0.01933	0.02416	0.02899	0.03382	0.03865

The friction factor is defined by the ratio of pressure drop and the kinetic energy of the fluid:

$$f = \frac{\Delta P}{(L/D_e)\rho V^2/2} \tag{4}$$

The overall thermo-hydraulic performance is evaluated by criterion *R3*, which is defined as the ratio of Nusselt numbers of an enhanced solar air heater and a smooth one under the same blowing energy consumption.

$$R3 = \frac{Nu}{Nu'} \tag{5}$$

where *Nu'* is the Nusselt number of the smooth duct which consumes blowing energy as much as the respective E-SAH does.

The relationship between the enhanced and the smooth ducts mentioned above can be written as:

$$f \times Re^3 = f' \times Re'^3 \tag{6}$$

and Filonenko equation [35],

$$f' = (1.82\lg Re' - 1.64)^{-2} \tag{7}$$

helps to find the values of Reynolds number of the smooth duct *Re'* through a MATLAB algorithm. The process is that: *Re* in Eq. (6) is the inlet boundary condition of studied solar collectors and *f* is calculated through Eq. (4), in which the pressure drop (ΔP) is obtained from the simulation results. Replace *f'* in Eq. (6) with the term at right side of Eq. (7), and a MATLAB algorithm is employed to work out *Re'*. Then, *Nu'* is calculated by Dittus-Boelter equation [36],

$$Nu' = 0.023 Re'^{0.8} Pr^{0.4} \tag{8}$$

Therefore, *R3* is found out to evaluate the overall performance of the enhanced solar air heaters.

2.5. Grid independence

Three models with different element numbers are tested to gain a set of grids dense enough. A simulation case is carried out with the amplitude, the attack angle and the number of arrangements being 2 mm, 45°, and 8 respectively with $Re = 18000$. The relative deviations for *Nu* and *f* are within ±0.85% and ±1.81% respectively between element numbers of 19×10^6 and 26×10^6 as shown in Table 4. So, the former mesh setting is considered dense enough to be applied to the rest cases in the present studies.

2.6. Model verification

Nusselt number and friction factor values of smooth duct determined from simulation results are compared with those evaluated by Dittus-Boelter equation (8) for *Nu* and Filonenko equation (7) for *f* to verify the reliability of present models [37]. Experimental data obtained by Sompol Skullong [17] is also employed to validate the numerical model, and an excellent agreement between simulation and experiment results is obtained.

Table 4
Grid independence verification for the simulations.

grid number	*Nu*	ε (%)	*f*	ε (%)
12 million	156.82	−1.15	0.1768	−4.22
19 million	158.65	−0.85	0.1846	−1.81
26 million	160.01	–	0.1880	–

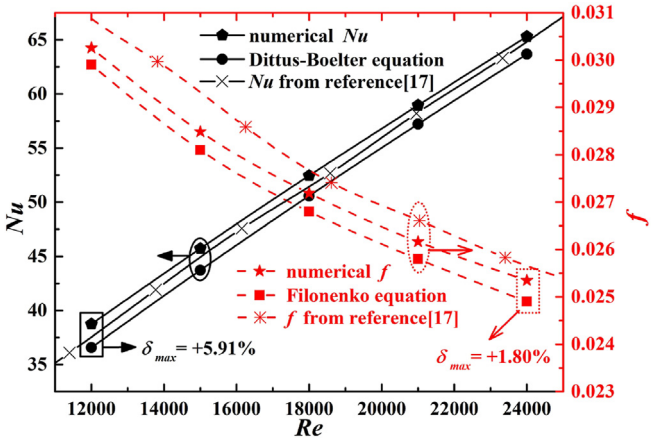

Fig. 5. Model verification for the *Nu* and *f* simulation results of the flat plate SAH.

As shown in Fig. 5, the relative deviations for Nusselt number between simulation results and experiment data are smaller than 3.04%, and that deviations between simulation results and the values predicted by Eq. (8) are smaller than 5.91%. Simultaneously, those deviations for friction factor are limited in −1.72% and 1.8% respectively. Thus, the present model has a reasonable calculation accuracy and is employed to finish the investigation.

3. Results and discussion

3.1. Flow structures

This section depicts the flow structures and analyzes the mechanism of heat transfer enhancement when air flows through the collectors. As a tool to realize visualization of the flow situations, streamlines are widely used in the post processing. Therefore, two bunches of streamlines of the air which flows through two adjacent grooves are shown in Fig. 6.

As the air flows through the inclined grooves, part of it near the ripple surface is induced by the grooves to deviate from the original flow direction. In the duct, a ripple surface is symmetrical to the adjacent ones, and this type of arrangement makes a couple of deviated flows near the heated surface collide with each other. Then the air rushes upwards to the bulk flow, generating a pair of longitudinal swirl flows. Meanwhile, the grooves lead to secondary flow in it as shown in Fig. 6.

CFD-Post is utilized to draw vortex core regions of the enhanced SAH with the parameters being $\alpha = 45°$, $A = 2$ mm and $N = 8$ when *Re* is 24000. Q-Criterion is a three-dimensional vortex criterion defining a vortex as a spatial region where,

$$Q = \frac{1}{2}\left[|\boldsymbol{\Omega}|^2 - |\boldsymbol{S}|^2\right] > 0 \tag{9}$$

where $\boldsymbol{S} = [\nabla v + (\nabla v)^T]/2$ is the rate-of-strain tensor, and $\boldsymbol{\Omega} = [\nabla v - (\nabla v)^T]/2$ is the vorticity tensor [38]. In this section, Q-Criterion is employed to judge the vortex situation. As shown in Fig. 7, the vortex cores are visualized when Q-Criterion is set as 0.025.

The strength level of the flow in the grooves is higher than 0.15, while that of longitudinal swirl flows is much weaker. The reason resulting the phenomenon is that the ripple surface has an impact on the air flow, generating secondary flows in the grooves, and then the inclined grooves induce the air to form longitudinal swirl flows with multi-vortex. The secondary flows are fed by the bulk flow and have a stronger vortices strength near the wall to reduce the temperature of the heated surface.

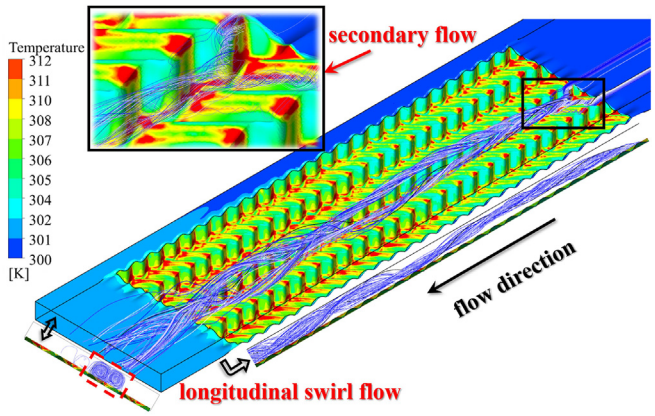

Fig. 6. Streamlines of the air flowing across a pair of inclined grooves.

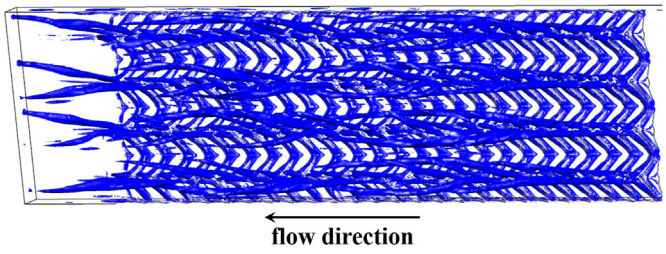

Fig. 7. The vortex core regions of secondary flows and the longitudinal swirls.

Some researchers installed criss-cross ribs to generate secondary flows near the heated wall to enhance heat transfer, and other researchers employed wings or winglets to form longitudinal vortices in the core region to mix working fluid. The novel contribution of this paper is the combination of both secondary flows near the boundary wall and longitudinal vortices in the core flow region to improve the performance of solar air heaters.

3.2. Heat transfer

The temperature contours of the collector walls and the cross-sections of the fluid along the flow direction are drawn in Fig. 8(a) and (b). The present cases are chosen when α, A, N, and Re are 45°, 2 mm, 8 and 24000, respectively. Air flows into the test section of the duct with uniform ambient temperature, 300K. Then, it is heated by the ripple surface with a uniform heat flux, 800W/m^2, resulting in the increase of the fluid temperature near the heated surface. A gust of hot air rising upwards exists near the places where a couple of adjacent grooves converge, meanwhile, the air with a low temperature flows downwards to the bottom surface and impinges on the other ends of the grooves as shown in Fig. 8(b).

The rising hot air forms mushroom-shaped temperature contours on the cross-sections, which intuitively demonstrate the mixing of the hot and the cold air in the solar air collectors. Heat transfer performance is poor at the ends of the grooves, as shown in Fig. 8(a), the reason of this phenomenon is that the air flows from the front side to the end side of grooves, and the secondary flows gradually became weaker in this process. With the increase of the ripple surface number (N), one, two, three and four mushroom-shaped contours are observed respectively and the SAH achieve more and more complete fluid mixing. The method of increasing the groove couples helps achieving larger turbulence kinetic energy (Fig. 8(c)) and more uniform temperature field in the bulk of the fluid (Fig. 12) and reducing the areas of the region with bad heat transfer performance (Fig. 8(a)). The longitudinal swirl flows make the temperature of the upper glass covers higher in Fig. 8(a). So, it is necessary to pack multi-glass covers on the E-SAHs to reduce the heat loss.

The heated ripple surface temperature is averaged along the

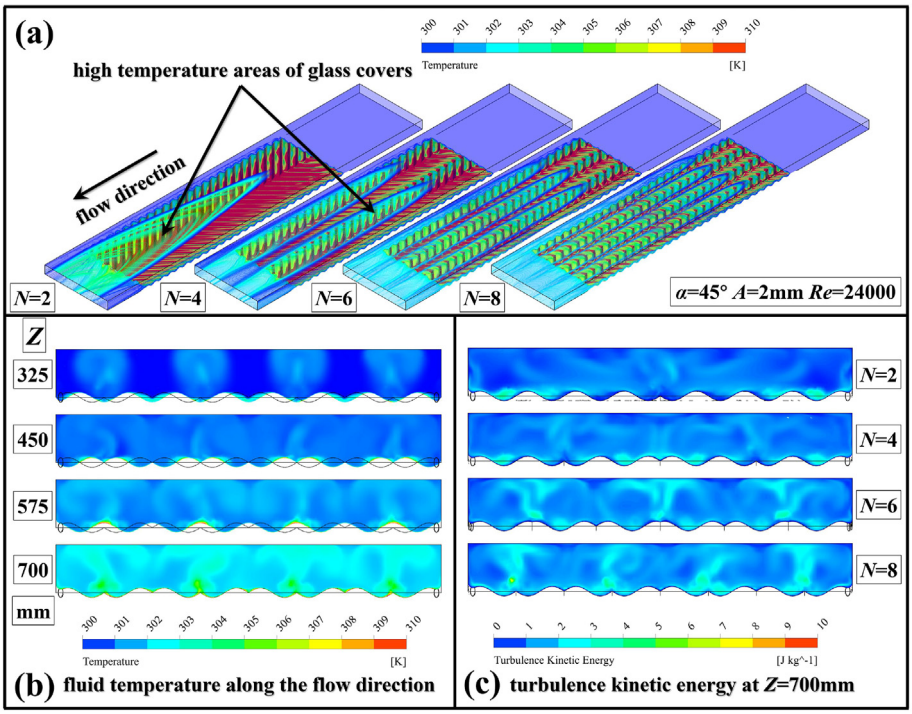

Fig. 8. Temperature of the collector walls (a) and the fluid sections (b) (C) turbulence kinetic energy at $Z = 700$ mm for SAHs with different N.

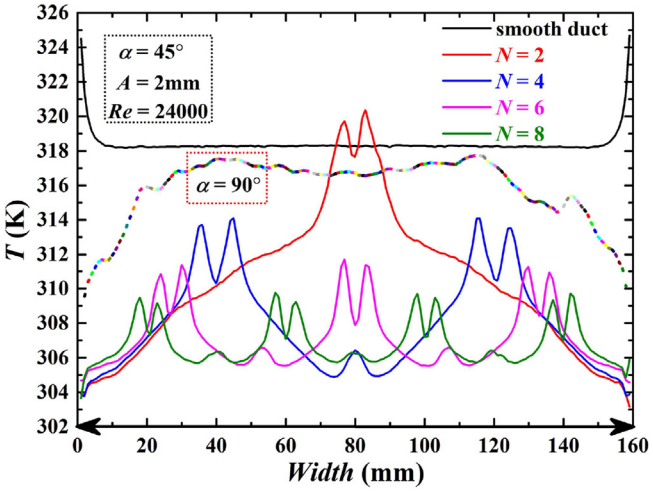

Fig. 9. Variation of the heated surface average temperature along the width.

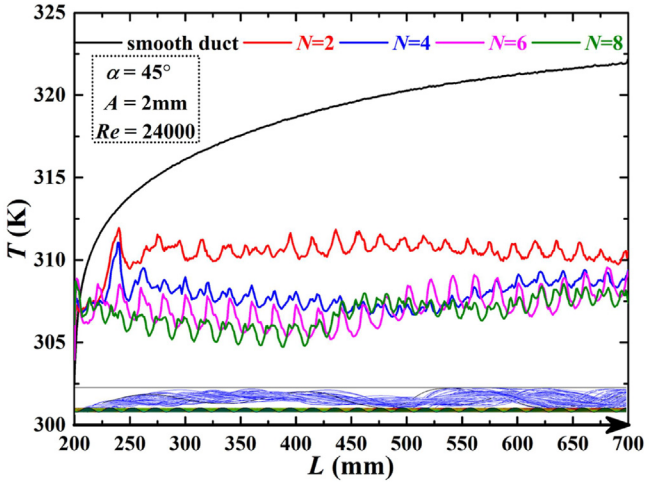

Fig. 10. The average temperature of the heated surfaces along the flow direction.

width of the mentioned ducts, the results are displayed in Fig. 9. Obviously, the smooth duct has a high uniform temperature distribution. The temperature increases rapidly near the two side surfaces due to the stagnation of the air. Enhanced solar air heaters obtain much lower average temperatures of heated surfaces. When α is 90°, which means the air flows across the grooves perpendicularly, the temperature near the side surfaces is considerably reduced. However, this type of surface is disable to reduce the temperature of the center region because there is no longitudinal swirl flow generated in the fluid filed. The inclined grooves with an attack angle of 45° can significantly reduce the temperature of heated surface as shown in Fig. 9 and therefore enhance the heat transfer process in the air ducts. Couples of double peaks occur in the temperature lines, representing the areas where heat transfer performance is obviously poor. The average temperature drops with the increase of number of the peaks.

Average temperature of the heated surfaces and the local Nusselt number along the flow direction are presented in Fig. 10 and Fig. 11 respectively. In the solar air heater with smooth duct, the temperature of the heated surface increases and the local Nusselt number decreases gradually along the flow direction, which means that a thermal boundary layer is developed while air flows through the test section. While in the enhanced solar air heaters, the wall

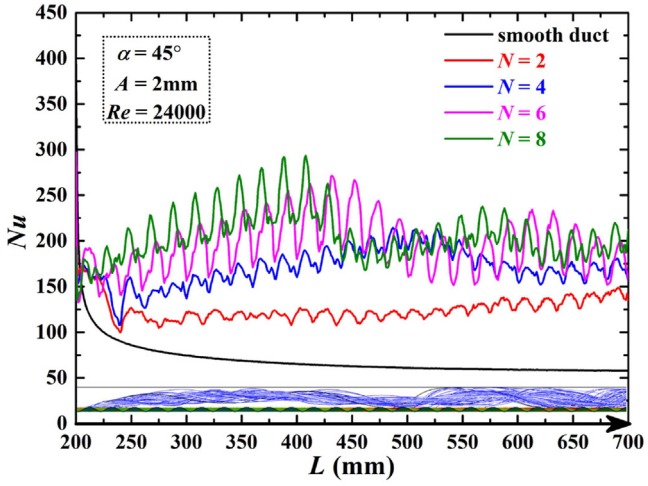

Fig. 11. Variation of Nusselt number along the flow direction.

temperatures are significantly reduced and the local Nusselt numbers are apparently enlarged compared to the SAH with smooth duct. Firstly, the secondary flows generated in the grooves break the thermal boundary layer, and secondly, the longitudinal vortices mix the hot fluid near the heated wall with the cold fluid in the core flow region. The waves of the *Nu* lines existing in Fig. 11 reveal that the windward areas, which is impinged by the working fluid directly, perform better than the leeward sides of the grooves.

Tangential streamlines and temperature contours of the cross-section are presented in Fig. 12. The parameters of the ducts are kept same as that mentioned before, and the *z* coordinate value of the section is 700 mm and that's the end side of the test section. A couple of longitudinal vortices flowing in opposite rotating directions are generated by a pair of adjacent grooves. As depicted before, the counter-rotating vortices carry the hot fluid away from the heated surfaces, and make the cold fluid to impinge the bottom surfaces of the collectors. With the increase of *N*, more counter-rotating vortices are generated, which contribute to achieve more sufficient mixing of the air in the core flow region.

The heat transfer performance of all the studied solar air heaters is depicted in Fig. 13 and Fig. 14, where convection heat transfer coefficient (h) ranges from 24W/(m^{2}K) to 140W/(m^{2}K) and *Nu* is short for the Nusselt numbers of the enhanced SAHs, while Nu_0 represents the Nusselt numbers of the smooth ducts which work under the same Reynolds number as the respective E-SAH does. It is observed that the E-SAHs obtain great improvement of heat transfer performance compared to the smooth ducts. When the attack angle is 90°, the ratio of *Nu* and Nu_0 is smaller than 1.22 for all the Reynolds numbers. The reason of the fact is that air flows across the grooves perpendicularly resulting poor heat transfer areas at the leeward sides of the grooves. There is no longitudinal vortex generated in the collector due to the grooves configuration which is perpendicular with the flow direction.

Obviously, the heat transfer is enhanced more when *N* increases from 2 to 8. A larger *N* means more longitudinal vortices which can make the air in the ducts mix more sufficiently and help to lower the wall temperature to reduce heat energy radiating from inside to the ambient. In most studied cases, Reynolds numbers of full turbulence have little effect on the *Nu* ratio. The ratio of Nusselt number increases with the decrease of the attack angle from 90° to 60° for $A = 1.5$ mm and 2 mm, and from 90° to 45° for $A = 1$ mm, reaching the maximum value around 3.3. When the attack angle decreases to 45° continually, there is no obvious heat transfer

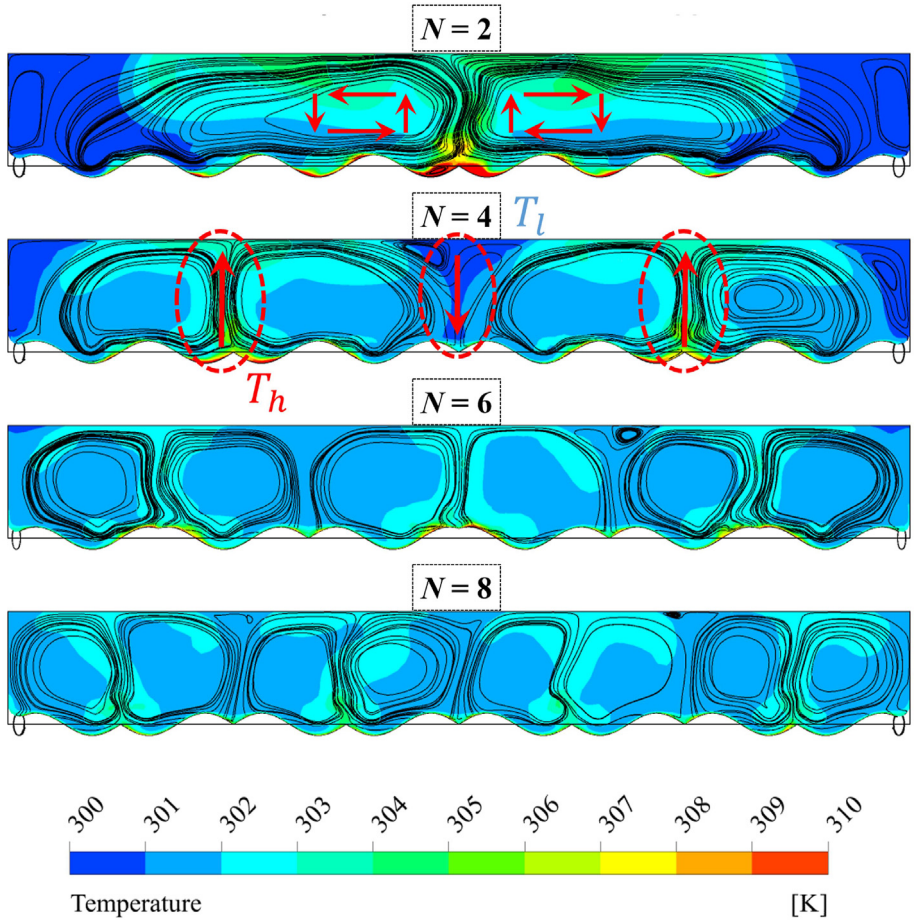

Fig. 12. The couple of the tangential streamlines and temperature.

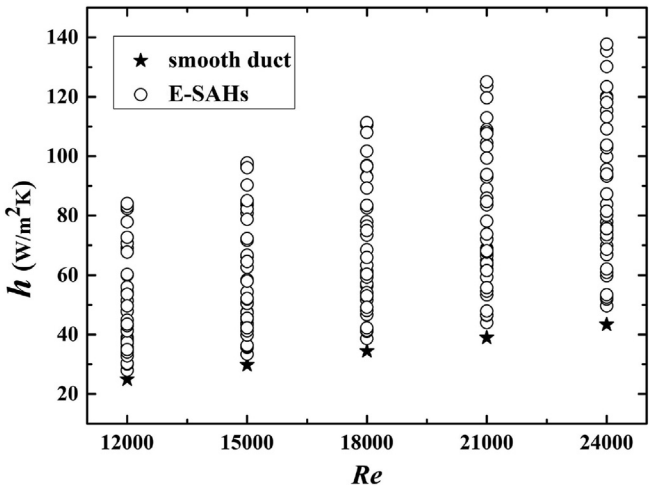

Fig. 13. Convection heat transfer coefficient of smooth duct and enhanced SAHs.

enhancement and even a slight decreasing tendency occurs in the ratio of Nusselt number for $A = 1.5$ mm and 2 mm. The reason for this phenomenon is that air tends to flow through the grooves fluently when the angle between the grooves and the flow direction becomes small enough. Meanwhile, the *Nu* ratio keeps growing with the inclining tendency of grooves in the present work when *A* is 1 mm. The deeper grooves generate stronger secondary flows and longitudinal vortices to give a much more significant improvement of the heat transfer performance. The maximum improvement of heat transfer, $Nu/Nu_0 = 3.38$, is obtained when $Re = 12000$ and the parameters are $A = 2$ mm, $\alpha = 45°$ and $N = 8$.

3.3. Pressure drops

The enhanced solar air collectors perform better in the heat transfer at the expense of more pressure drop. When air flows through the test section, secondary flows are generated in the inclined grooves, improving the heat transfer and establishing longitudinal swirl flows to mix the air with different temperature. The secondary flows and the counter-rotating vortices can increase the friction dissipation of the fluid, and result in much more impingement between the air and the collector surfaces. Therefore, enhanced solar air collectors consume more blowing energy than the smooth one under the same Reynolds number.

The ratio of friction factors between E-SAHs and smooth collectors, f/f_0, where f_0 represents the friction factor of smooth collector under the same *Re* as E-SAHs work at, is displayed in Fig. 15. The variety of the ratio of friction factors is similar with that of Nusselt number. As shown in Fig. 15, when the parameter *A* is 1.5 mm or 2 mm, the ratio f/f_0 increases with the decrease of the attack angle from 90° to 60° and then decreases with the continue decrease of the attack angle. The air flows along the grooves more fluently resulting in much weaker friction and impingement when the grooves are inclined enough. In most cases, a larger *N* and deeper grooves increase more energy consumption because there

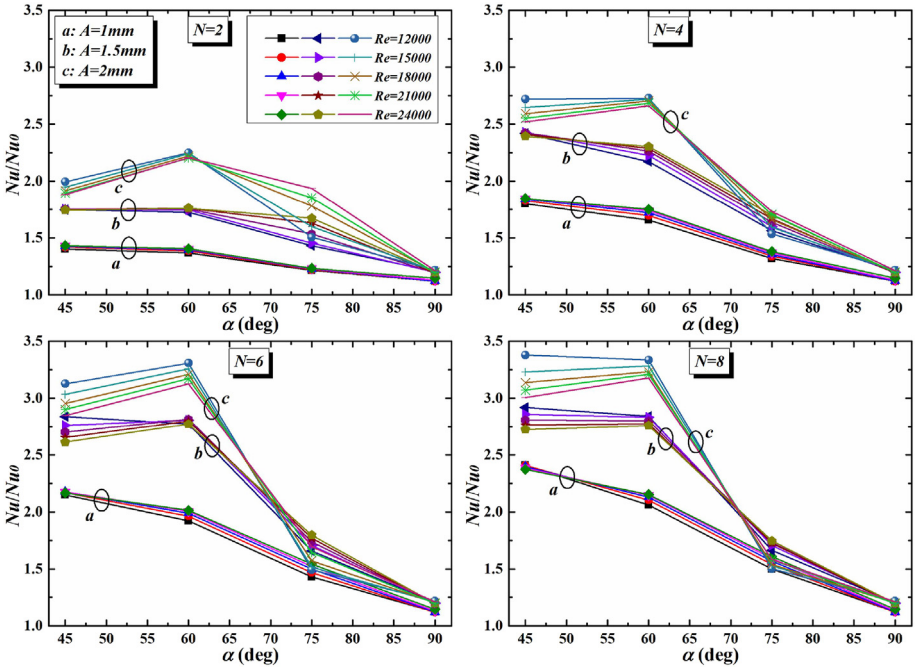

Fig. 14. The variation of the ratio of the Nusselt number.

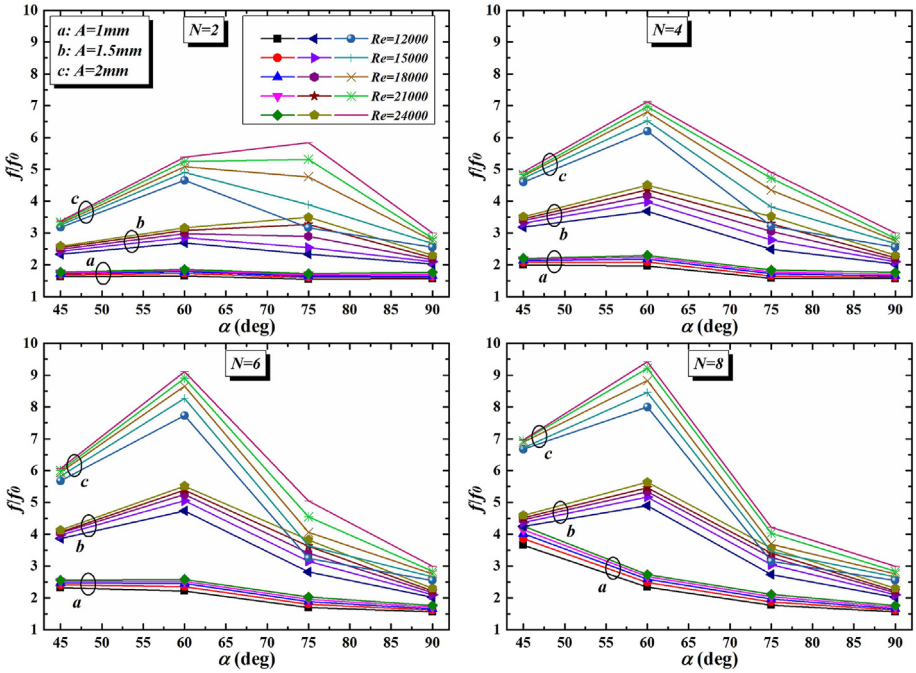

Fig. 15. The variation of the ratio of the friction factor.

are stronger secondary flows and more longitudinal vortices generated in the ducts causing more inner flowing friction. Maximum ratio of friction factor, $f/f_0 = 6.96$, occurs when A, α, N and the Reynolds number are 2 mm, 45°, 8 and 24000, respectively.

3.4. Overall thermo-hydraulic performance

R3, which reveals the heat transfer ability of E-SAHs compared with the smooth one under the same energy consumption, is applied to evaluate the overall thermo-hydraulic performance of E-SAHs. The effect of parameters on the comprehensive performance is displayed in Fig. 16. *R3* is smaller than 1 when air flows across the grooves perpendicularly ($\alpha = 90°$), which means that the E-SAH with straight grooves performs worse overall heat transfer performance than the SAH with smooth duct under the same blowing energy consumption. Due to lack of longitudinal vortices, straight grooves improve heat transfer performance less than that inclined grooves do.

The enhanced solar air heaters composed with inclined ripple surfaces behave much better. Generally, *R3* increases with the

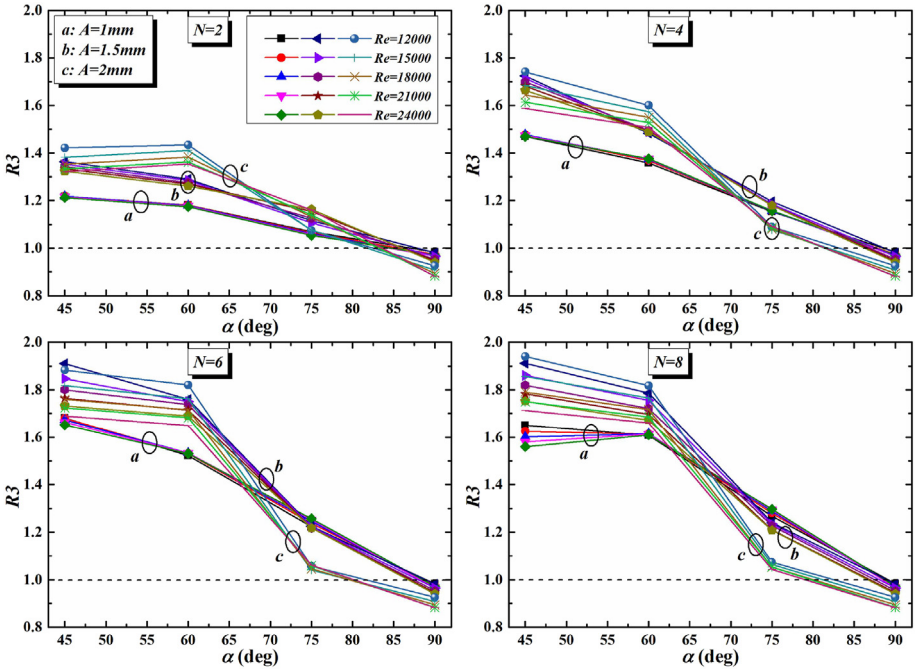

Fig. 16. The overall thermo-hydraulic performance.

decrease of the attack angle and the increase of *N*. As depicted in Fig. 16, the deeper grooves ($A = 2$ mm) result in better comprehensive performance with the smaller attack angles ($\alpha = 60°$ and 45°) but behave worse when α is large. Grooves with smaller α induce air to establish stronger longitudinal vortices to mix bulk flow sufficiently, causing high performance of heat transfer.

Different arrangement numbers, *N*, are investigated. In the most cases, the E-SAHs with more counter-rotating vortices perform better. For the collectors with shallow grooves ($A = 1$ mm), *R3* has a nearly free relationship with Reynolds number. While, *R3* decreases with the growing of *Re* for deeper grooves in small attack angles, but this *R3* difference is not obvious and the effect of *Re* on the overall performance can be ignored because the air flows as full turbulence under all Reynolds numbers studied.

The best comprehensive performance, $R3 = 1.94$, is achieved when α, *A*, *N* and *Re* are respectively 45°, 2 mm, 8 and 12000. That means this enhanced solar air heater improves the heat transfer ability by around 94% than smooth one under the same blowing energy consumption.

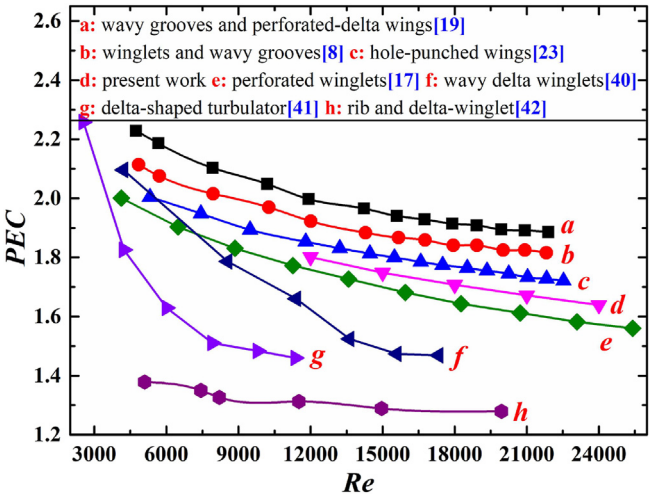

Fig. 17. Comparison of present and previous works [8,17,19,23,40–42].

3.5. Comparison with previous works

Lots of similar research has been carried out by many researchers and another criterion, which is defined as $PEC = \frac{Nu/Nu_0}{(f/f_0)^{1/3}}$, is widely used to evaluate the overall thermo-hydraulic performance of the enhanced solar air heaters [39].

A comparison of *PEC* values between present and previous work is depicted in Fig. 17. When *Re* ranges from 12000 to 24000, the E-SAHs composed with inclined ripple surface improve heat transfer efficiency with a moderate frictional penalty, obtaining the fourth-best overall thermal-hydraulic performance. Therefore, it is significant to investigate this type of air collector and the technique has a great potential to improve the performance of the heaters to collect thermal energy with higher quality.

4. Conclusions

A numerical investigation is conducted in this paper, giving an analysis of the enhanced solar air heaters composed with inclined ripple surface which has three different parameters, groove depth (*A*), attack angle (α), surface array number (*N*). Flow structures and thermo-hydraulic characteristics are also analyzed, and the following conclusions are obtained based on the simulation results:(1) When the air flows through the enhanced solar air heaters, secondary flows are generated in the grooves and then induced to establish longitudinal swirl flows with multiple counter-rotating vortices in the core region. The combination of secondary flows and longitudinal vortices is the novel contribution of this paper and the it is proved this flow structure mixes the fluid completely and perform well in the heat transfer augmentation with a moderate increase of pressure drop. The convection heat transfer coefficient was enhanced from 24W/(m^{2}K) to maximum 140W/(m^{2}K).(2) The inclined grooves improve the ability of heat transfer by 1.21–3.38

times than smooth duct and induce more dissipation of mechanical energy, which is revealed by the increase of friction factor, ratio of which is from 1.54 to 6.96. In most cases, the deeper grooves give larger heat transfer augmentation and consume more blowing energy. When the angle is small enough, air flows along the grooves fluently, making weaker secondary flows so that insignificant enhancement on heat transfer is obtained. (3) The overall thermo-hydraulic performance of the collectors with straight grooves is much worse, *R3* is smaller than 1, while the inclined grooves behave well to improve the heat transfer performance by 94% to the greatest extent under same blowing energy consumption. Generally, the overall characteristics increase with the increase of the array number of the grooves, whose optimal value is around 6 or 8. There is an optimal attack angle around 45°–60°. When *N* is 6 or 8, α is 60° or 45°, the enhanced solar air heaters perform 50%–94% better than smooth duct under same mechanical energy consumption. The best thermo-hydraulic performance, $R3 = 1.94$, occurs when *A* is 2 mm, attack angle is 45°, *N* is 8 and Reynolds number is 12000 and that's the best parameter composition to make the solar air heaters perform well.

CRediT authorship contribution statement

Zhimin Dong: directed the research and wrote the essay. **Peng Liu:** helped to fix some of the errors; And, Prof. Zhichun Liu and Prof. Wei Liu supported this job. **Hui Xiao:** helped to fix some of the errors; And, Prof. Zhichun Liu and Prof. Wei Liu supported this job.

Declaration of competing interest

The authors declare that they have no known competing financial interests or personal relationships that could have appeared to influence the work reported in this paper.

Acknowledgments

The present study is supported by the National Natural Science Foundation of China (No. 51736004 and No. 51776079).

Nomenclature

A	groove depth, mm
D_e	equivalent diameter of duct, mm
f	friction factor
h	convection heat transfer coefficient, W/(m^2•K)
H	height of duct, mm
L	length of duct, mm
Nu	Nusselt number
N	number of groove arrays
PEC	performance evaluation criterion
ΔP	pressure drop, Pa
Pr	Prandtl Number
Q	heat flux, W/m^2
R3	overall thermo-hydraulic performance criterion
Re	Reynolds number
T	temperature, K
T_w	wall temperature, K
T_m	average temperature of air, K
V	fluid velocity, m/s
W	width of duct, mm
x, *y*, *z*	Cartesian coordinates

super/subscripts

'	smooth duct under same blowing energy consumption
0	smooth duct under same Reynolds numbers

Greek symbols

α	attack angle, °
κ	thermal conductivity of fluid, W/(m·K)
μ	dynamic viscosity, kg/(m·s)
ρ	fluid density, kg/m^3

References

[1] W. Fuqiang, C. Ziming, T. Jianyu, Y. Yuan, S. Yong, L. Linhua, Progress in concentrated solar power technology with parabolic trough collector system: a comprehensive review, Renew. Sustain. Energy Rev. 79 (2017) 1314–1328.
[2] W. Fuqiang, M. Lanxin, C. Ziming, T. Jianyu, H. Xing, L. Linhua, Radiative heat transfer in solar thermochemical particle reactor: a comprehensive review, Renew. Sustain. Energy Rev. 73 (2017) 935–949.
[3] S.A. Kalogirou, Solar thermal collectors and applications, Prog. Energy Combust. Sci. 30 (3) (2004) 231–295.
[4] A. Kumar, M.-H. Kim, Convective heat transfer enhancement in solar air channels, Appl. Therm. Eng. 89 (2015) 239–261.
[5] B. Bhushan, R. Singh, A review on methodology of artificial roughness used in duct of solar air heaters, Energy 35 (1) (2010) 202–212.
[6] R.P. Saini, J. Verma, Heat transfer and friction factor correlations for a duct having dimple-shape artificial roughness for solar air heaters, Energy 33 (8) (2008) 1277–1287.
[7] A.S. Yadav, J.L. Bhagoria, A numerical investigation of square sectioned transverse rib roughened solar air heater, Int. J. Therm. Sci. 79 (2014) 111–131.
[8] S. Skullong, P. Promvonge, C. Thianpong, N. Jayranaiwachira, M. Pimsarn, Heat transfer augmentation in a solar air heater channel with combined winglets and wavy grooves on absorber plate, Appl. Therm. Eng. 122 (2017) 268–284.
[9] T. Alam, M.-H. Kim, Heat transfer enhancement in solar air heater duct with conical protrusion roughness ribs, Appl. Therm. Eng. 126 (2017) 458–469.
[10] G. Xie, S. Zheng, W. Zhang, B. Sundén, A numerical study of flow structure and heat transfer in a square channel with ribs combined downstream half-size or same-size ribs, Appl. Therm. Eng. 61 (2) (2013) 289–300.
[11] P. Singh, Y. Ji, S.V. Ekkad, Experimental and numerical investigation of heat and fluid flow in a square duct featuring criss-cross rib patterns, Appl. Therm. Eng. 128 (2018) 415–425.
[12] M.-A. Moon, M.-J. Park, K.-Y. Kim, Evaluation of heat transfer performances of various rib shapes, Int. J. Heat Mass Tran. 71 (2014) 275–284.
[13] W. Liu, P. Liu, J.B. Wang, N.B. Zheng, Z.C. Liu, Exergy destruction minimization: a principle to convective heat transfer enhancement, Int. J. Heat Mass Tran. 122 (2018) 11–21.
[14] J. Wang, W. Liu, Z. Liu, The application of exergy destruction minimization in convective heat transfer optimization, Appl. Therm. Eng. 88 (2015) 384–390.
[15] A. Bejan, Fundamentals of exergy analysis, entropy generation minimization, and the generation of flow architecture 26 (7) (2002), 0-43.
[16] H. Xiao, J. Wang, Z. Liu, W. Liu, Turbulent heat transfer optimization for solar air heater with variation method based on exergy destruction minimization principle, Int. J. Heat Mass Tran. 136 (2019) 1096–1105.
[17] S. Skullong, P. Promthaisong, P. Promvonge, C. Thianpong, M. Pimsarn, Thermal performance in solar air heater with perforated-winglet-type vortex generator, Sol. Energy 170 (2018) 1101–1117.
[18] S. Tamna, S. Skullong, C. Thianpong, P. Promvonge, Heat transfer behaviors in a solar air heater channel with multiple V-baffle vortex generators, Sol. Energy 110 (2014) 720–735.
[19] S. Skullong, P. Promvonge, C. Thianpong, M. Pimsarn, Thermal performance in solar air heater channel with combined wavy-groove and perforated-delta wing vortex generators, Appl. Therm. Eng. 100 (2016) 611–620.
[20] S. Skullong, S. Kwankaomeng, C. Thianpong, P. Promvonge, Thermal performance of turbulent flow in a solar air heater channel with rib-groove turbulators, Int. Commun. Heat Mass Tran. 50 (2014) 34–43.
[21] S. Skullong, P. Promvonge, Experimental investigation on turbulent convection in solar air heater channel fitted with delta winglet vortex generator, Chin. J. Chem. Eng. 22 (1) (2014) 1–10.
[22] S. Skullong, C. Thianpong, P.J.H. Promvonge, M. Transfer, Effects of rib size and arrangement on forced convective heat transfer in a solar air heater channel 51 (10) (2015) 1475–1485.
[23] P. Promvonge, S. Skullong, Heat transfer augmentation in solar receiver heat exchanger with hole-punched wings, Appl. Therm. Eng. 155 (2019) 59–69.
[24] D. Jin, S. Quan, J. Zuo, S. Xu, Numerical investigation of heat transfer enhancement in a solar air heater roughened by multiple V-shaped ribs, Renew. Energy 134 (2019) 78–88.
[25] D. Jin, M. Zhang, P. Wang, S. Xu, Numerical investigation of heat transfer and fluid flow in a solar air heater duct with multi V-shaped ribs on the absorber plate, Energy 89 (2015) 178–190.
[26] W. Liu, P. Liu, Z.M. Dong, K. Yang, Z.C. Liu, A study on the multi-field synergy principle of convective heat and mass transfer enhancement, Int. J. Heat Mass Tran. 134 (2019) 722–734.
[27] P. Liu, N. Zheng, F. Shan, Z. Liu, W. Liu, Numerical study on characteristics of heat transfer and friction factor in a circular tube with central slant rods, Int. J. Heat Mass Tran. 99 (2016) 268–282.
[28] M. Sheikholeslami, S.A. Farshad, A. Shafee, H. Babazadeh, Performance of solar

collector with turbulator involving nanomaterial turbulent regime, Renew. Energy 163 (2021) 1222–1237.
[29] M. Sheikholeslami, M. Jafaryar, Z. Said, A.I. Alsabery, H. Babazadeh, A. Shafee, Modification for helical turbulator to augment heat transfer behavior of nanomaterial via numerical approach, Appl. Therm. Eng. 182 (2021) 115935.
[30] M. Sheikholeslami, M. Jafaryar, A. Shafee, Z. Li, R.-u. Haq, Heat transfer of nanoparticles employing innovative turbulator considering entropy generation, Int. J. Heat Mass Tran. 136 (2019) 1233–1240.
[31] M. Sheikholeslami, R. Ellahi, Three dimensional mesoscopic simulation of magnetic field effect on natural convection of nanofluid, Int. J. Heat Mass Tran. 89 (2015) 799–808.
[32] W. Gao, W. Lin, T. Liu, C. Xia, Analytical and experimental studies on the thermal performance of cross-corrugated and flat-plate solar air heaters, Appl. Energy 84 (4) (2007) 425–441.
[33] S. Singh, Experimental and numerical investigations of a single and double pass porous serpentine wavy wiremesh packed bed solar air heater, Renew. Energy 145 (2020) 1361–1387.
[34] H. Buchberg, D.K. Edwards, Design considerations for solar collectors with cylindrical glass honeycombs, Sol. Energy 18 (3) (1976) 193–203.
[35] R. Raj, N.S. Lakshman, Y. Mukkamala, Single phase flow heat transfer and pressure drop measurements in doubly enhanced tubes, Int. J. Therm. Sci. 88 (2015) 215–227.
[36] F. Dittus, L. Boelter, Heat transfer in automobile radiators of the tubular type, Int. Commun. Heat Mass Tran. 12 (1) (1985) 3–22.
[37] F.P. Incropera, D.P. DeWitt, T.L. Bergman, A.S. Lavine, F.P. Incropera, Foundations of Heat Transfer, Wiley Textbooks2012.
[38] G. Haller, An objective definition of a vortex, J. Fluid Mech. 525 (2005) 1–26.
[39] R.L. Webb, Performance evaluation criteria for use of enhanced heat transfer surfaces in heat exchanger design, Int. J. Heat Mass Tran. 24 (4) (1981) 715–726.
[40] J.S. Sawhney, R. Maithani, S. Chamoli, Experimental investigation of heat transfer and friction factor characteristics of solar air heater using wavy delta winglets, Appl. Therm. Eng. 117 (2017) 740–751.
[41] M.T. Baissi, A. Brima, K. Aoues, R. Khanniche, N. Moummi, Thermal Behavior in a Solar Air Heater Channel Roughened with Delta-Shaped Vortex Generators, Applied Thermal Engineering, 2019.
[42] P. Promvonge, C. Khanoknaiyakarn, S. Kwankaomeng, C. Thianpong, Thermal behavior in solar air heater channel fitted with combined rib and delta-winglet, Int. Commun. Heat Mass Tran. 38 (6) (2011) 749–756.